SAND2015-2156C

Dynamic Wake Meandering Model Comparison with Varying Fidelity Models for Wind Turbine Wake Prediction

Brandon L. Ennis
Senior Member of the Technical Staff
Sandia National Laboratories
Albuquerque, NM, USA

Christopher L. Kelley
Senior Member of the Technical Staff
Sandia National Laboratories
Albuquerque, NM, USA

David C. Maniaci
Senior Member of the Technical Staff
Sandia National Laboratories
Albuquerque, NM, USA

ABSTRACT

The dynamic wake meandering model (DWM) is a common wake model used for fast prediction of wind farm power and loads. This model is compared to higher fidelity vortex method (VM) and actuator line large eddy simulation (AL-LES) model results. By looking independently at the steady wake deficit model of DWM, and performing a more rigorous comparison than averaged result comparisons alone can produce, the models and their physical processes can be compared. The DWM and VM results of wake deficit agree best in the mid-wake region due to the consistent recovery prior to wake breakdown predicted in the VM results. DWM and AL-LES results agree best in the far-wake due to the low recovery of the laminar flow field AL-LES simulation. The physical process of wake recovery in the DWM model differed from the higher fidelity models and resulted solely from wake expansion downstream, with no momentum recovery up to 10 diameters. Sensitivity to DWM model input boundary conditions and their effects are shown, with greatest sensitivity to the rotor loading and to the turbulence model.

NOTATION

a	disk-averaged axial induction
b_{95}	95% wake width
C_D	wake drag coefficient
D	wind turbine rotor diameter
n_d	number of downstream locations
$n_{d,r}$	number of radial positions and downstream location, d
R	wind turbine rotor radius
STE_c	standard error for case, c
STE_d	standard error for downstream position, d
TI_{amb}	atmospheric turbulence intensity
U	streamwise velocity
U_{amb}	freestream ambient velocity
$U_{def,min}$	minimum velocity in the wake plane of interest
$\overline{U}_{d,r}^{DWM}$	streamwise velocity at point r at downstream location d for the DWM model
$\overline{U}_{d,r}^{model}$	streamwise velocity at point r at downstream location d for the higher fidelity model
U_∞	freestream ambient velocity
u'	turbulent streamwise fluctuating velocity
$\overline{u'v'}$	Reynold's shear stress
V_r	radial velocity
v'	turbulent radial fluctuating velocity
ν_T	Eddy viscosity

Presented at the AHS 71st Annual Forum, Virginia Beach, Virginia, May 5–7, 2015. This work was funded by the United States Government's Department of Energy and is not subject to copyright protection in the U.S.

INTRODUCTION

The shift from a single turbine design approach towards an integrated systems wind farm design process depends upon the availability of accurate and fast wind turbine wake models. Wind plant control algorithms based on power performance and loads optimization can be designed using high-fidelity wake models, but in-field implementation will require the ability to rapidly predict power and loads using high-efficiency wake models. This paper will compare three common models with differing levels of fidelity for predicting wake flow downstream of a wind turbine; the wake model used in the Dynamic Wake Meander (DWM) model an engineering model, a free-wake vortex method model and Actuator Line Large Eddy Simulation (AL-LES) model.

The DWM model is a commonly used wake prediction tool for design and analysis of wind farms developed by Madsen and Larsen in 2003 (Ref. 1). The model combines three modules for (1) calculating a steady wake deficit, (2) rotor added turbulence using the Mann model and (3) including the effects of wake meandering to shift the downstream quasi-steady wake based on the turbulent length scales. A good description of each of these modules is provided by Madsen (Ref. 2). Recent updates have been performed by Keck on this model including: revision of the turbulence model to incorporate a 2-d viscosity model (Ref. 3), inclusion of the effects of atmospheric shear and better model turbulence far downstream (Ref. 4), and incorporation of the effects of atmospheric stability (Ref. 5).

Verification of the DWM model has been illustrated historically through comparison with AL-LES simulations to com-

pare predicted wake deficit shape (radial dependence) and evolution downstream (axial dependence). Madsen showed DWM predictions matching well with the ELLIPSYS3D AL-LES model, with increasing deviation to the wake shape at further distances downstream (greater than 6 diameters) and increasing turbulence (greater than 5%) (Ref. 2). The error with downstream prediction of wake shape is improved by Keck's implementation of a 2-d viscosity as shown in comparison with AL-LES predictions of the same wind turbine (Ref. 3). The effect of an atmospheric stability correction was seen to improve the model predictions compared to OpenFOAM AL-LES with more noticeable effects downstream where wake meandering is more pronounced (Ref. 5). These results are validated using data from the North Hoyle wind farm for three stability classes at spacing's of 11, 10, and 4.4 diameters downstream, showing particularly good agreement for the unstable atmospheric state for the five turbines in the row at the larger spacing's.

Validation cases have been performed using the DWM model and AL-LES to compare to wind turbine performance and meteorological tower measurements within large wind farms. Churchfield compared DWM with OpenFOAM AL-LES predictions of the Egmond aan Zee offshore wind farm (Ref. 6).

DWM power prediction comparison with experimental data at different spacing's for rows of up to 12 wind turbines produced agreement within one standard deviation of the experimental data. The case that was afforded to compare AL-LES predictions had better power prediction using the DWM model, although the AL-LES loads predictions is in better agreement with the data. Hao compared predictions from OpenFOAM AL-LES to DWM and showed exceptional agreement with the normalized power from experimental results into the fifth row (Ref. 7). Despite the agreement for power predictions, an underprediction of turbine loads was seen as shown by Churchfield (Ref. 6) but reduced with an enhanced wake meandering model. The simulations were compared to data from Lillgrund wind farm where the power prediction error was around 5% for the first 5 rows and increased to 10% in deeper rows. Keck showed the validity of the DWM model in comparison with data at Lillgrund and Horns Rev wind farms for normalized power predictions at downstream turbines, with overall differences on the order of 5% (Ref. 8). Larsen compared DWM predictions with measurement at the Egmond aan Zee wind farm for loads and power over the 360° wind sector with good agreement (Ref. 9).

This paper seeks to add to the existing literature an analysis which looks at the details of performance of the steady wake deficit model within the DWM. Much attention has been given to the overall model and comparing it with averaged results as a measure of performance, but this paper takes a more focused study of one component of the DWM, the wake deficit model. By comparing the physics between the models, and looking at unsteady results understanding can be gained as to why or why not the model works well. In cases where DWM does work well it should be ensured that it's not just a result of two equal and opposite error sources.

METHODS

In this paper three computational methods of modeling the wake behind a wind turbine are used to predict the performance of the same concept wind turbine and to compare the results. The wind turbine design is described by Kelley, named "Design A (Ref. 10)." The models compared all have different assumptions and varying levels of modeling, with increasing fidelity as introduced below. From low to high fidelity, the model domain takes minutes to hours, days, and up to weeks for one simulation for these three codes. Description of the models compared and some background into each follows in this section.

Dynamic Wake Meander Wake Deficit Model

The DWM wake deficit model is one of the three modules of the complete DWM model, each applied independently as additive steps. In this paper the steady wake deficit prediction of the DWM model is used alone in comparison with the other wake models. Rotor added turbulence does not affect the driving wake deficit model, but rather is superimposed upon it, and is therefore not relevant in comparing a single wake calculation. Additionally, the meandering model changes the average wake in the presence of turbulent length scales greater than twice the rotor diameter. The present comparison is for laminar inflow, and meandering in this model therefore does not come into play.

The steady wake deficit model within DWM was first proposed for use in describing a wind turbine by Ainslie in 1988 (Ref. 11). The wake is modeled using a thin shear-layer solution of the Navier-Stokes equations which assumes steady, incompressible and axisymmetric flow with pressure terms neglected and that gradients are much greater in the radial direction than in the axial direction. This wake deficit model, from here on used interchangeably with "DWM model" for simplification, then uses an Eddy Viscosity turbulence model, ν_T, of the Reynolds shear stress term to achieve turbulence closure. The incompressible form of the continuity equation is used to relate the radial velocity to the solution axial velocity. The form of the Navier-Stokes equations for this model is greatly simplified in this approach and can be solved rapidly using a numerical grid on a personal computer. The fundamental equations of the DWM wake deficit are then derived, shown in Equations 1-3.

$$U\frac{\partial U}{\partial x}+V_r\frac{\partial U}{\partial r}=-\frac{1}{r}\frac{\partial}{\partial r}(r\overline{u'v'}) \tag{1}$$

$$-\overline{u'v'}=\nu_T\frac{\partial U}{\partial r} \tag{2}$$

$$\frac{\partial U}{\partial x}+\frac{1}{r}\frac{\partial}{\partial r}rV_r=0 \tag{3}$$

These governing equations are known to be incomplete representations of the physics for an actual wind turbine, but

chosen to reduce computational demands of the solution so the model can be used to make controls decisions or in iterative wind farm design processes. The Eddy viscosity term in the DWM model is the mechanism for addressing the model assumptions and calibrating the solution, and its formulation has seen numerous changes since the DWM model development in 2003 (Ref. 1). The term is calculated to include superposition of turbulence contribution arising from (1) the wake shear layer and from (2) incoming turbulence due to the atmosphere. These two components are both traditionally calibrated to a "true" value, typically assumed from an AL-LES model. The Eddy viscosity term has been adjusted from the original one-dimensional form that varied with axial distance, Equation 4, to a two-dimensional version which better represents the physical phenomena occurring in the turbulence generation from the wake shear, Equation 5, to an atmospheric shear-adjusted form, Equations 6-8. It is noted that details of the shear adjusted Eddy viscosity model are overlooked but can be found with rigorous explanation (Ref. 5).

$$\nu_{T,\,Madsen\ 2010} = F_1 k_1 T I_{amb} + F_2 k_2 b (U_{amb} - U_{def,min}) \quad (4)$$

$$\nu_{T,\,Keck\ 2012} = F_1 k_1 T I_{amb} + F_2 k_2 b^2 \left|\frac{\partial U}{\partial r}\right| \frac{1}{U_{amb} R} \quad (5)$$

$$\nu_{T,\,Keck\ 2013} = \nu_{T,\,Keck\ 2012} \frac{\frac{\partial U}{\partial r}_{Total}}{\left|\frac{\partial U}{\partial r}_{DWM}\right|} \quad (6)$$

$$\frac{\partial U}{\partial r}_{Total} = \frac{A_{Total}}{2\pi} \quad (7)$$

$$A_{Total} = \begin{cases} 2\pi \frac{\partial U}{\partial r}_{DWM} & \text{if, } \left|\frac{\partial U}{\partial r}\right| \geq \frac{\partial U}{\partial z}_{ABL}. \\ 2\pi \frac{\partial U}{\partial r}_{DWM} + 2A_{1,2} & \text{if, } \left|\frac{\partial U}{\partial r}\right| < \frac{\partial U}{\partial z}_{ABL}. \end{cases} \quad (8)$$

In this analysis, the maximum of the 1-d and 2-d formulation of the Eddy viscosity models is used at each grid point. The 2-d formulation is highest everywhere in the domain except for occasionally in the innermost region of the wake. The filters, F_i, describe the axial distribution of turbulence generation. To correct for the model assumption of zero pressure gradients, F_1 describes the pressure recovery which is traditionally assumed to occur at 2 diameters downstream based on work by Sanderse (Ref. 12). F_2 is then incorporated to calibrate for the turbulence development in the wake. The calibration parameters, k_i, are constants that scale the amount of turbulence contribution from the two sources. The calibration parameters incorporated into the two-dimensional Eddy viscosity formulation by Keck are repeated in this analysis. The calibration constants used are k_1 = 0.0914 and k_2 = 0.0216, with filter functions as shown in Figure 1 (Ref. 3).

The solution from the DWM model is obtained using 2nd order central differencing in the radial direction and 1st order

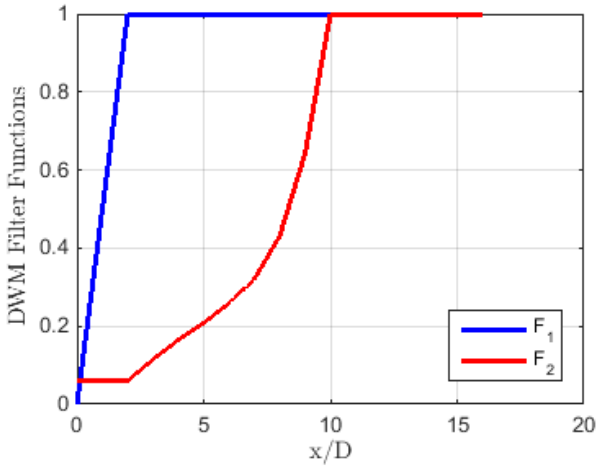

Fig. 1. DWM Eddy Viscosity Filter Values.

forward differencing in the axial direction. The averaged rotor loading profile is input as the boundary condition with no radial flow at the rotor disk. As an attempt to adjust for the model inability to treat pressure recovery from the wake, the rotor loading is assumed to start at the 1-d analysis far-field, full recovery value of twice the rotor induction. The fully-expanded velocity at the rotor plane is used, however without adding in rotor expansion, as described by Keck for the 2-d Eddy viscosity formulation (Ref. 3). The solution is marched downstream by solving for the axial velocity at the adjacent downstream section using the momentum equation with Eddy viscosity and then using the continuity equation to solve for the radial velocity, which is a decoupled step in the solution.

Free-Wake Vortex Method

Lagrangian vortex methods (VM) are mid-fidelity models capable of directly predicting wake structure and development downstream, but at a significantly lower cost than with conventional CFD. The Code for Axial and Cross-flow TUrbine Simulation (CACTUS) is a three-dimensional free-wake vortex filament code developed at Sandia National Laboratories for the study of vertical- and horizontal-axis wind turbines (Ref. 13). Wind turbine blades are modeled using a lifting line approximation with the blades discretized into blade elements each containing a bound vortex line. These vortex lines are shed from the blade related to the change in bound circulation on the blade, and propagate downstream to freely interact, generating the wake structure. The velocity field induced by the entire vortex system is calculated using the Biot-Savart law. The wake affects the local induced velocity on the blades, which is used to determine relative flow angle and to obtain the local circulation from lookup of airfoil data tables. This iterative process is repeated to convergence, and then the wake can be averaged for meaningful statistics.

The CACTUS simulation was performed with 20 time steps per revolution, corresponding to a time step of Δt=0.07 sec, and results shown are for the "Design A" sim-

ulation (Ref. 10). The simulation was run for 120 revolutions with time-averaged and fluctuating quantities determined from averaging revolutions 80 through 120.

Actuator-Line Large Eddy Simulation Model

Large Eddy Simulation is a high-fidelity CFD model that solves the three-dimensional, unsteady, spatially-filtered Navier-Stokes equations. The actuator-line method represents the blades as rotating lines with distributed forces calculated from local flow angle and airfoil table lookup. This representation of the blade eliminates the need for the grid to be resolved into the boundary layer of the airfoil since the effect of the blades on the flow is represented by their body forces and not geometry.

The Virtual Wind Simulator (VWiS) AL-LES code developed at the University of Minnesota is used to compare with the other models using the simulation performed by Yang (Ref. 14). The simulation was run with a computational domain of 8Dx8Dx18D with 300 million grid points, corresponding to a uniform nodal resolution of 200/diameter in the turbine plane. The simulation time averaged the final 50 turbine revolutions after the kinetic energy statistically reached steady state.

Analysis Methods

The wake evolution will be described by the integral wake momentum deficit of the flow relative to freestream. This is derived as follows in Equations 9-13. A control volume analysis is performed with an expanding streamtube which contains the wind turbine as the outer boundary. The linear momentum and continuity equations combine to produce the drag force which is non-dimensionalized as shown in Equation 11. The final equation will be used to describe wake recovery and physically means the amount of drag imposed on the fluid within the control volume at $U = U(x)$.

$$-\int_{A_i} \rho \vec{U}_\infty \left| \vec{U}_\infty \cdot d\vec{A}_i \right| + \int_{A_e} \rho \vec{U} \left| \vec{U} \cdot d\vec{A}_e \right| = -D \tag{9}$$

$$-\int_{A_i} \rho \left| \vec{U}_\infty \cdot d\vec{A}_i \right| + \int_{A_e} \rho \left| \vec{U} \cdot d\vec{A}_e \right| = 0 \tag{10}$$

$$D = \int_{A_e} \rho U (U_\infty - U)\, dA_e \tag{11}$$

$$C_D = \frac{2\pi \int_0^{r_e} \rho U (U_\infty - U) r\, dr}{\frac{1}{2}\rho U_\infty^2 \pi R^2} \tag{12}$$

$$C_D = 4 \int_0^{r_e/R} \frac{U}{U_\infty} \left(1 - \frac{U}{U_\infty}\right) \left(\frac{r}{R}\right) d\left(\frac{r}{R}\right) \tag{13}$$

Wake recovery at a given position is also aided by expansion of the wake downstream. This expansion is quantified using a wake width parameter, b_{95}. This parameter describes the radius of the wake containing 95% of the mass deficit from freestream, Equations 14-15.

$$U_{def,total} = 2\pi \int_0^\infty \left(1 - \frac{U}{U_\infty}\right) \left(\frac{r}{R}\right) d\left(\frac{r}{R}\right) \tag{14}$$

$$b_{95} = r\,(0.95\, U_{def,total}) \tag{15}$$

Error will be quantified between model predictions using the standard error approach in Equation 16, as used by Keck (Ref. 3). This is a sum of squares error calculation that looks at the difference in predictions for each radial location, r, at each downstream position, d, for one (or a sum of) atmospheric cases of freestream velocity and atmospheric turbulence, c.

$$STE_c = \sqrt{\frac{1}{n_d} \sum_{d=1}^{n_d} \left(\frac{1}{n_{d,r}} \sum_{r=1}^{n_{d,r}} \left(\overline{U}_{d,r}^{model} - \overline{U}_{d,r}^{DWM} \right)^2 \right)} \tag{16}$$

RESULTS

Model Inputs

Prior to a direct comparison of the results, it is necessary to compare the actual rotor boundary condition. The DWM model requires as input the disk-averaged axial induction, which will serve as the comparison between the three models' rotor boundary conditions. Comparison of the resultant axial induction profile is determined from the velocity field at the rotor plane for VWiS and CACTUS, and is shown in Figure 2. Although the planform and airfoil data tables used by the actuator line implementation in both the AL-LES and VM models was identical, the resultant induction profile is substantially different. This discrepancy is due to a "performance tip loss model" implemented in the AL-LES method, which is multiplied with the actuator line body forces imposed onto the LES domain (Ref. 15). This model is used to account for pressure roll-off at the blade tip, which causes formation of the tip vortex and reduces outboard loading. At a tip speed ratio of 9 this model has a significant effect resulting in much of the rotor loading discrepancy between the two models. This discrepancy unfortunately limits the ability for a direct comparison of the two models, so rather, qualitative conclusions will be drawn from this analysis and where applicable the DWM will be used to match either of the rotor loading profiles for direct comparison.

Steady Results

In the literature, the DWM model has been shown to perform especially well at moderate distances downstream, but in some cases with increased deviation beyond 6 diameters (Ref. 2). The results of the axial wake deficit evolution downstream and radial velocity along radial planes are shown in Figure 3, to compare the predictions of the three models.

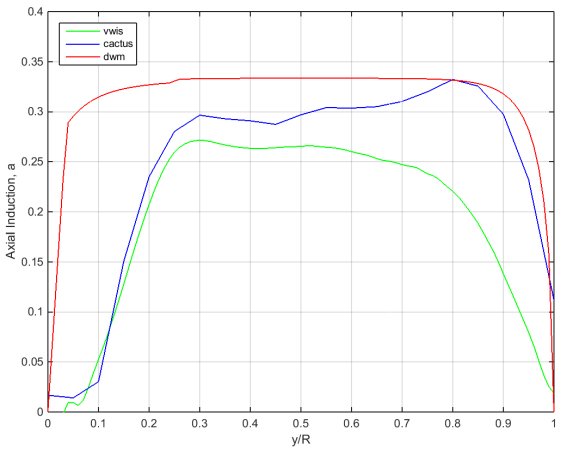

Fig. 2. Rotor Resultant Axial Induction for the Three Models.

When not considering meandering and turbulence generation, the DWM model produces a steady prediction that is compared with the averages of these parameters for the two unsteady models. This comparison highlights the areas where the models agree and disagree, but is not sufficient for understanding the physical cause that is driving the discrepancy. In past studies comparisons were performed looking at steady averages only. The averaged results are sufficient for comparing to experimental data, which is typically from 10-minute averaged SCADA data, but yields no further insight into what modeling assumptions are driving discrepancies.

Steady axial velocity deficit is compared along downstream planes in Figure 3A, revealing the wake evolution predictions from the three models. The rotor plane location, $x/D = 0$, shows the boundary condition for the DWM model which is taken as twice the rotor induction of the disk-averaged performance, $U_{BC} = U_{amb}(1-2a)$. The point of "DWM model validity" is typically assumed to begin at 3 diameters, where the near-wake pressure field and swirl velocity are close to zero as modeled by the DWM model. For the laminar flow-field chosen in this analysis the far-wake transition would be expected to occur later than with atmospheric turbulence. An apparent discrepancy in the steady results is the inner-wake at 1 diameter where the higher fidelity models both have accelerated flow greater than the freestream velocity, due to the lack of a nacelle model used by either method. The hub vortices produced by this increased shear will then be stronger than realistic and drive the wake to a quicker recovery as the vortex system merges closer to the turbine. The final disclaimer to comparing the results is that the rotor loading profile is different between the three models as discussed earlier, and is essentially comparing three different rotors. This discrepancy will be addressed later in this section. With these model and setup discrepancies noted, the comparison that follows should be taken as mostly qualitative.

Comparison of DWM with CACTUS results reveals good agreement beginning at 4 diameters downstream and continuing to 7 diameters where the CACTUS prediction begins to recover more quickly. The CACTUS result is seen to recover most quickly between the three models which is an interesting result for this inviscid, potential flow solution. The near-wake model of DWM seems to transition between 4-5 diameters downstream, as would be expected from the zero turbulence flowfield.

The AL-LES code, VWiS, is seen to recover slowest in this comparison, and even at 10 diameters downstream has yet to reach the self-similar velocity profile characterizing the far-wake regime. VWiS is in agreement with CACTUS predictions up to 3 diameters downstream, but then CACTUS begins to recover quickly and better match the DWM predictions. There appears to be a significant difference in wake stability in the inner-wake region near the hub between these two higher fidelity models driving the large discrepancies far downstream.

Averaged radial velocity shown along radial planes is compared between the three models in Figure 3B. Results here show a high radial velocity at the rotor plane due to the pressure-driven flow blockage caused by the rotor accelerating flow around the rotor. Radial velocity as high as 25% of the freestream value is seen at the rotor tip in the higher fidelity models. The standard DWM model assumes a zero radial velocity profile at the rotor which is obviously incorrect as seen in this comparison. This is a simple thing to add in the DWM model, and effects of this addition will be discussed later in this paper. The radial velocity planes from the CACTUS results show instability starting in the inner-wake at 2 diameters downstream and this is a result of large vortical structure meandering, and the radial velocity would likely go to zero similar to VWiS given sufficient averaging.

Model agreement for wake axial velocity prediction is described numerically using the standard error formula of Equation 16 by looking at each downstream location, d, individually. This comparison should remain qualitative but the STE values enable a clearer comparison between the model predictions and their regions of agreement. Taking 10% error as "good" agreement, the results discussed above are seen numerically where DWM agreement with CACTUS results occurs between 4-7 diameters and with VWiS between 6-10 diameters. It is difficult from this comparison to say which model prediction DWM agrees best with, but it is noted that the input rotor loading boundary condition is most different between DWM and VWiS. In the furthest downstream locations the agreement between DWM and CACTUS has less error than the agreement between CACTUS and VWiS, showing that the DWM prediction in this region is between the two higher fidelity models where CACTUS recovers quicker and VWiS slower.

With the trends for wake deficit evolution from the model predictions shown and compared, it is now the objective to explain their source. There are two main mechanisms for wake recovery, (1) diffusion from vortex generation and inflow turbulence and (2) wake expansion driven by the shear layer between the wake and freestream. The diffusion contribution is

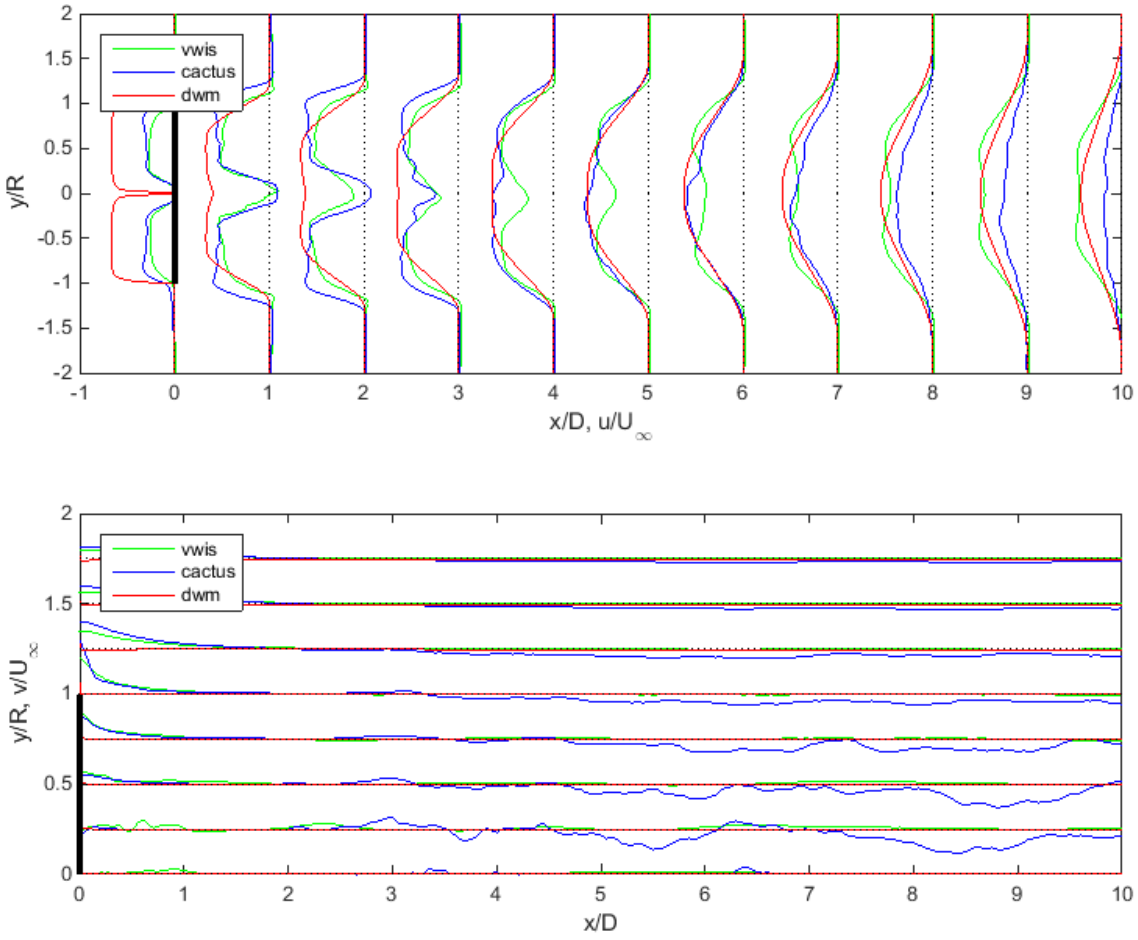

Fig. 3. Averaged (A) Axial and (B) Radial Velocity Planes.

quantified by calculating the total momentum flux through a streamtube containing the wind turbine at points downstream to describe the net momentum deficit of the turbine and its wake, Equation 13. The wake expansion contribution to wake recovery is described by the 95% wake width formulation, Equation 15, which is the radius of the wake whose area contains 95% of the mass deficit.

Momentum deficit of the turbine and its wake is shown in Figure 5 for the three models. At some point far downstream you would expect to see full momentum recovery from the freestream, and by 10 diameters downstream there is significant momentum recovery for CACTUS, and VWiS is beginning to recover from the peak drag of the wake which occurs around 8 diameters. The DWM result does not show momentum recovery at 10 diameters. The momentum recovery is due to mixing and dissipation and this result shows that CACTUS results contain the most mixing and dissipation in this laminar inflow case between the models.

The calculated wake width produced from the three models is shown in Figure 6. From this figure the CACTUS and VWiS results appear to be very similar in terms of the wake outer boundary spreading. DWM however does not agree well with the other methods and the wake width spreads nearly 50% by 10 diameters downstream.

Considering the results for these two wake recovery parameters, it is clear that the DWM model recovers from wake expansion, CACTUS recovers most significantly due to momentum diffusion, and VWiS has similar wake expansion as CACTUS but with far less momentum recovery.

Unsteady Results

In order to truly understand the physical reasons for discrepancies between the DWM and higher fidelity models it is necessary to look at the unsteady results which drive the steady performance. As mentioned, in the DWM this process is simply modeled by the Eddy viscosity and its filters and calibration constants. The eddy viscosity for the DWM model is formulated to replace the turbulent Reynold's shear stress, $\overline{u'v'}$.

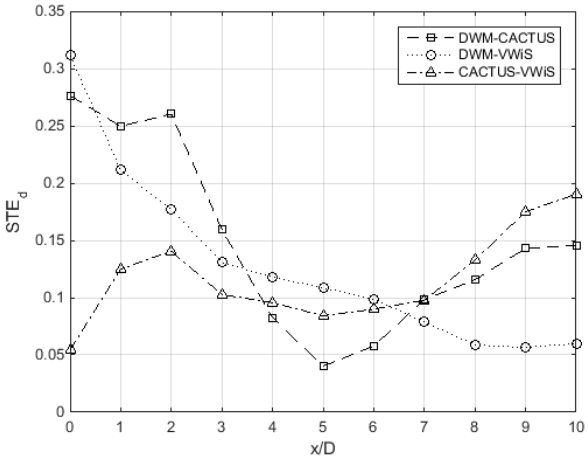

Fig. 4. Standard Error Between Models at Downstream Planes.

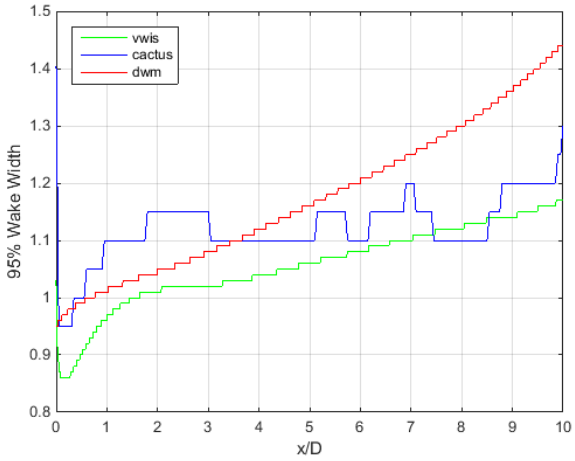

Fig. 6. Model 95% Wake Deficit, Wake Width (line integral).

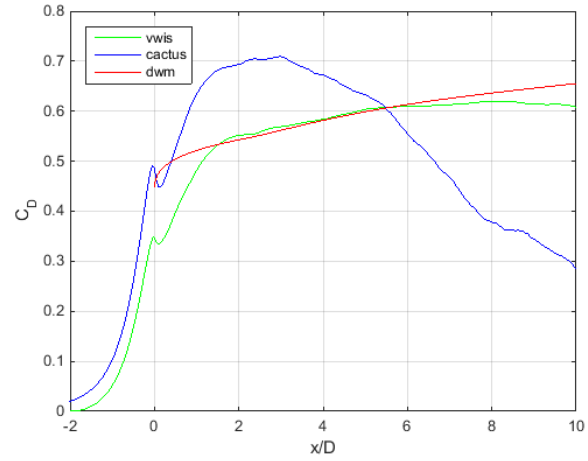

Fig. 5. Averaged Wake Radial Velocity.

Reynold's shear stress and in overall wake recovery.

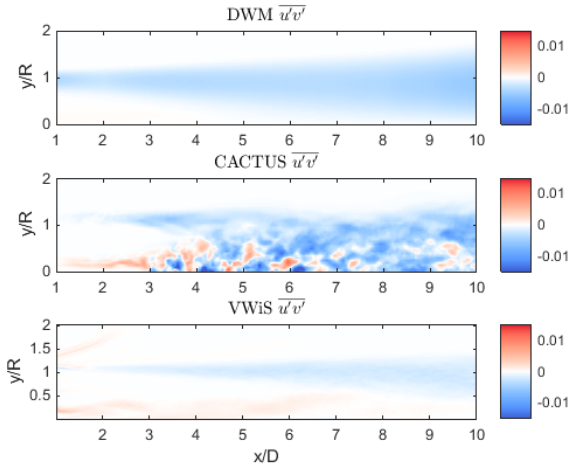

Fig. 7. Averaged Reynold's Shear Stress Comparison.

Comparison of this averaged Reynold's stress for the higher fidelity models is made with the DWM output Reynold's shear field and shown in Figure 7.

There are a few interesting conclusions to be drawn from this comparison. The overall patterns of the Reynold's shear are similar amongst the models, but the CACTUS results are clearly not sufficiently averaged with the 40 revolutions averaging scheme. Additionally, you can see the same trend in this property as with model recovery, where CACTUS has the highest values for the Reynold's stress, then DWM, then VWiS. The shear layer appears to reach the centerline quickest for CACTUS implying the shortest transition to the far-wake. In this shear layer region values for the three models are approximately $\overline{u'v'}$ = -0.004 for DWM, -0.006 for CACTUS and -0.002 for VWiS. It is also worth noting that instantaneous vorticity is not compared in this analysis as the AL-LES method resulted in only small scale vorticity and not the large, coherent vortices seen with wind turbine wakes. This difference in wake structure may be what drove the differences in

DWM Performance with Improved Boundary Conditions

As described earlier, the errant boundary conditions used to describe the wind turbine rotor make it difficult to compare the models quantitatively. This section will look at the effect of using more accurate boundary conditions on the DWM model agreement with the higher fidelity models. The summary of this comparison, along with the boundary conditions used, is shown in Table 1. For this analysis, sensitivity to correct axial induction, input radial velocity profile, and eddy viscosity is shown for the two comparisons of DWM with the higher fidelity models. In these columns, the BC derived from the comparison model results is fed in as input to the DWM model. The comparison in this table is done in terms of the standard error equation, STE_c, between the higher fidelity models and the DWM model with matching boundary

conditions. This error is calculated within the region of DWM validity assumed to start at 3 diameters downstream. The sensitivity to these boundary conditions appears to be most significant for axial induction and then for matching the correct Eddy viscosity. The change in Eddy viscosity was done to match the higher fidelity model and was performed by multiplying the k_2 scaling constant to add 33% for comparison to CACTUS and reduce by 33% for comparison to VWiS. In future studies this boundary condition will be applied by direct input of the Reynold's shear stress, $\overline{u'v'}$, into the governing equations eliminating the need for an Eddy viscosity model.

Table 1. DWM Model Boundary Condition Sensitivity .

DWM BC	DWM-CACTUS	DWM-VWiS
Original Design (Fig. 2)	0.086	0.077
Matched Induction, a	0.079	0.076
Matched a, V_r	0.079	0.074
Matched a, V_r, ν_T	0.073	0.065

[a](Comparison shown in model comparison of STE_c)

From Table 1 it is seen that the addition of the radial velocity boundary condition has little effect on the final accuracy of the wake prediction. The reasoning for the negligible effect of this BC can be observed in Figure 8. While the radial and axial velocity are coupled in the DWM analysis, the radial velocity is forced to zero much more rapidly than for the higher fidelity models. Essentially the effect of this BC for DWM is small and contained within 0.05 x/D.

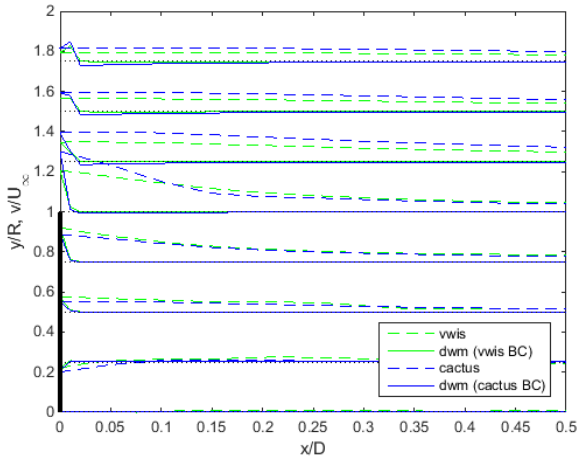

Fig. 8. Radial Velocity Boundary Condition Evolution.

As a final comparison of the discrepancy between the model predictions and DWM, Figure 9 shows the standard error values comparing the models with the correct boundary conditions. The same trend is seen as before, but with reduced bias between the compared models.

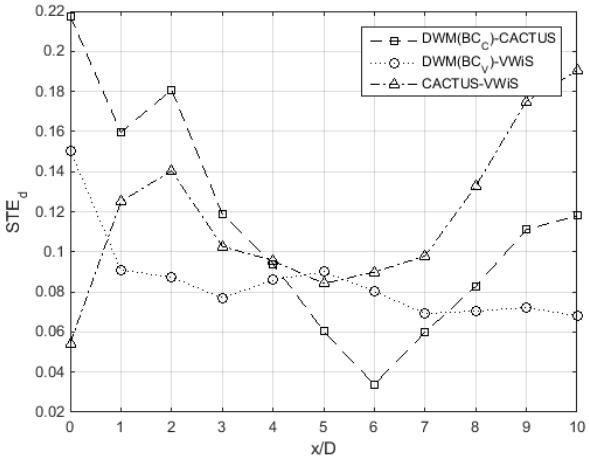

Fig. 9. Standard Error when Matching the Boundary Conditions.

CONCLUDING REMARKS

In this paper a method was shown for comparing high fidelity, time accurate models with the Dynamic Wake Meander (DWM) model. Direct, quantitative comparison could not be made due to the discrepancy in the boundary condition (BC) between the CACTUS Vortex Method (VM) model and VWiS Actuator Line Large Eddy Simulation (AL-LES), so conclusions are left as qualitative metrics. In this comparison it was found that the VM was most predictive of the mid-wake shape and velocity deficit (4-7 diameter downstream), while AL-LES predictions were closest to DWM in the far-wake (8-10 diameter). Although the velocity difference across the downstream planes is small between AL-LES and DWM, the velocity deficit shape from the AL-LES model is displaying near-wake qualities at up to 10 diameters due to the very low dissipation of this model implementation. The two higher fidelity models actually have the largest discrepancy from each other in the far-wake due to the observed differences in momentum diffusion and the rotor BC.

Sensitivity to boundary conditions of the DWM model was studied and it was observed that having the correct disk-averaged axial induction BC holds the most significance on solution convergence. Changing the Eddy viscosity value through a multiplication factor to the turbulence generated in the wake shear layer also had a significant effect in this study, where a 33% change to the k_2 calibration constant produced about a 10% reduction in model discrepancies. The ideal way to check the sensitivity of the model discrepancies to the Eddy viscosity model would be to recalibrate the DWM model to both of the higher-fidelity models and affect the spatial representation of the Eddy viscosity through the F_2 filter. In this paper a clear error was seen from assuming the radial velocity profile at the rotor plane was zero; however, using the velocity profile at the rotor as an input to DWM had the smallest effect on improving the model discrepancy with DWM. This is probably due to the DWM model assumptions driving this radial velocity to zero much more quickly than seen in the VM

or AL-LES models. When changing the DWM boundary conditions to more accurately represent the other models a noted improvement in the total wake error was seen on the order of 15-20%.

While the DWM model did agree with VM and AL-LES results over specific regions of the wake, the wake development was seen to be driven through different mechanisms. The VM model recovered back towards freestream quickest due to a very rapid momentum recovery. The DWM wake prediction recovered second quickest but due entirely to a 45% wake expansion and at 10 diameters downstream had yet to see any momentum recovery. The AL-LES results had a small amount of momentum recovery and 15% wake expansion, similar to the VM expansion, and recovered the least in this comparison. The trend in wake recovery could have been predicted by comparing the magnitude of the averaged Reynold's shear stress, $\overline{u'v'}$. This physical quantity in the governing equations of DWM is the complete representation of turbulence after model assumptions, and appears to serve as a good comparison of the turbulence generation in the wake that drives wake recovery.

Further analysis is needed to draw significant conclusions with model instances which are more consistent in their representation of the wind turbine rotor as designed, which is typical of the classic wind turbine design. Future work is recommended and will follow this study to compare DWM results without using the Eddy viscosity model but rather with direct input of the actual Reynold's shear from the "true" solution. This input of the averaged CACTUS and averaged VWiS cases can be used to determine if you can reproduce that model's steady wake deficits more precisely. This comparison will reveal the significance of other DWM model assumptions when given the exact value for turbulence dissipation as modeled. To study the surprisingly high momentum recovery of the VM prediction, future studies are recommended with various turbulence levels to determine which is most representative of the VM result. A means of quantifying the near-wake contribution to error in the model comparison should also be studied in future work. A proposed method is to perform a Proper Orthogonal Decomposition (POD) of time accurate results on cross-wake planes at different downstream locations to reveal shape modes and their significance to the averaged result. This would reveal how the energy gets distributed across the modes with distance downstream until far-wake similarity is observed.

Author contact: Brandon L. Ennis, blennis@sandia.gov.

ACKNOWLEDGMENTS

The authors would like to acknowledge Xiaolei Yang, Aaron Boomsma, and Prof. Fotis Sotiropoulos from the University of Minnesota for their excellent work in obtaining the cases from their VWiS AL-LES code, having this data as a benchmark for the other models has been critical. The authors also recognize Yujia Hao and Prof. Matthew Lackner from the University of Massachusetts Amherst for their assistance in getting a version of the DWM model written in house. This work is funded by the U.S. Department of Energy's National Nuclear Security Administration under contract DE-AC04-94AL85000, (SAND2014-4643 A).

REFERENCES

[1]Madsen, H. A., Thomsen, K. and Larsen, G. C., "A New Method for Prediction of Detailed Wake Loads," Proceedings of the IEA Joint Action of Wind Turbines 16th Symposium, 2003, S.-E. Thor, ed., pp. 171-188.

[2]Madsen, H. A., Larsen, G. C., Larsen, T. J., Troldberg, N. and Mikkelson, R., "Calibration and validation of the Dynamic Wake Meandering model implemented in the aeroelastic code HAWC2," *Journal of Solar Energy Engineering*, Vol. 132, (4), 2010, pp. 041014-1–041014-14.

[3]Keck, R.-E., Veldkamp, D., Madsen, H. A. and Larsen, G., "Implementation of a Mixing Length Turbulence Formulation Into the Dynamic Wake Meandering Model," *Journal of Solar Energy Engineering*, Vol. 134, (2), 2012, pp. 021012-1–021012-13.

[4]Keck, R.-E., de Mare, M., Churchfield, M. J., Lee, S., Larsen, G. and Madsen, H. A., "Two improvements to the dynamic wake meandering model: including the effects of atmospheric shear on wake turbulence and incorporating turbulence build-up in a row of wind turbines," *Journal of Wind Energy*, 2013.
doi: 10.002/we.1686

[5]Keck, R.-E., de Mare, M., Churchfield, M. J., Lee, S., Larsen, G. and Madsen, H. A., "On atmospheric stability in the dynamic wake meandering model," *Journal of Wind Energy*, 2013.
doi: 10.1002/we.1662

[6]Churchfield, M. J., Moriarty, P. J., Hao, Y., Lackner, M. A., Barthelmie, R., Lundquist, J. K. and Oxley, G.S., "A Comparison of the Dynamic Wake Meandering Model, Large-Eddy Simulation, and Field Data at the Egmond aan Zee Offshore Wind Plant," Paper AIAA 2015-0724, 33rd ASME Wind Energy Symposium, Kissimmee, FL, January 5–9, 2015.

[7]Hao, Y., Lackner, M. A., Keck, R.-E., Lee, S., Churchfield, M. J. and Moriarty, P., "Implementing the Dynamic Wake Meandering Model in the NWTC Design Codes,", Paper AIAA 2014-1089, 32nd ASME Wind Energy Symposium, National Harbor, MD, January 13–17, 2014.

[8]Keck, R.-E., "Validation of the standalone implementation of the dynamic wake meandering model for power production," *Journal of Wind Energy*, 2014.
doi: 10.1002/we.1777

[9]Larsen, T. J., Madsen, H. A., Larsen, G. C. and Hansen, K. S., "Validation of the dynamic wake meander model for loads and power production in the Egmond aan Zee wind farm," *Journal of Wind Energy*, Vol. 16, 2013, pp. 605–624.
doi: 10.1002/we.1563

[10]Kelley, C. L., Maniaci, D. C. and Resor, B. R., "Horizontal-Axis Wind Turbine Wake Sensitivity to Different Blade Load Distributions," Paper AIAA 2015-0490, 33rd ASME Wind Energy Symposium, Kissimmee, FL, January 5–9, 2015.

[11]Ainslie, J. F., "Calculating the Flow Field in the Wake of Wind Turbines," *Journal of Wind Engineering and Industrial Aerodynamics*, Vol. 27, 1988, pp. 213–224.

[12]Sanderse, B., "Aerodynamics of Wind Turbine WakesLiterature Review," Technical Report No. ECN-E-09-016, 2009.

[13]Murray, J. C. and Barone, M., "The Development of CACTUS, a Wind and Marine Turbine Performance Simulation Code," AIAA 49th Aerospace Sciences Meeting, Vol. 147, 2011.

[14]Yang, X., Boomsma, A. and Sotiropoulos, F., "Effects of blade spanwise load distribution on turbine wake development," Paper AIAA 2015-0492, 33rd ASME Wind Energy Symposium, Kissimmee, FL, January 5–9, 2015.

[15]Shen, W. Z., Mikkelson, R. and Sorenson, J. N., "Tip Loss Corrections for Wind Turbine Computations," *Journal of Wind Energy*, Vol. 8, 2005, pp. 457–475.
doi: 10.1002/we.153